

<sup>16</sup>We have implicitly assumed that the transverse momentum of the gluon fragmentation is small compared to that of the bremsstrahlung effect. Otherwise, gluon jets would be even harder to detect. It has even been speculated that gluon jets may not exist. See, e.g.,

G. L. Kane and Y.-P. Yau, University of Michigan Report No. UM-HE-77-44, 1977 (to be published).

<sup>17</sup>S. J. Brodsky, D. G. Coyne, T. A. DeGrand, and R. R. Horgan, Phys. Lett. **73B**, 203 (1978); M. Kramer and H. Krasemann, Phys. Lett. **73B**, 58 (1978).

## Average Lifetimes of Collective Transitions in the Spin-(30-50) Region

H. Hübel,<sup>(a)</sup> U. Smilansky,<sup>(b)</sup> R. M. Diamond, and F. S. Stephens

*Lawrence Berkeley Laboratory, University of California, Berkeley, California 94720*

and

B. Herskind

*The Niels Bohr Institute, University of Copenhagen, Copenhagen, Denmark*

(Received 1 August 1978)

A method is developed to determine average lifetimes of continuum gamma rays following heavy-ion compound-nucleus reactions. The resulting enhancement factors for  $E2$  transitions depopulating states in the spin-(30-50) regions are of the same order of magnitude as for ground-state rotational bands of deformed nuclei. This shows for the first time that these high-spin states decay through strongly collective bands.

The de-excitation  $\gamma$ -ray spectra of nuclei produced at very high angular momenta in heavy-ion compound-nucleus reactions are composed of three parts.<sup>1</sup> The intensity of the high-energy part of the spectra ( $E_\gamma \gtrsim 1.5$  MeV for deformed nuclei in the heavy rare-earth region) falls exponentially with  $E_\gamma$ . In this region the angular correlation is roughly isotropic, suggesting about equal amounts of dipole and quadrupole transitions.<sup>2,3</sup> Furthermore, the multiplicity associated with each transition is roughly independent of  $E_\gamma$ . This part of the spectrum is very likely produced by statistical transitions. The low-energy region of the spectrum ( $\leq 0.7$  MeV) is dominated by discrete lines, the transitions between the well-separated and strongly populated low-energy states. In this paper, we will focus our attention on the intermediate range of  $\gamma$ -ray energies where the spectrum shows a broad structure (the "bump") with the following characteristics:

(i) The multiplicity of transitions at the high-energy edge of the bump is higher than the average multiplicity associated with either the statistical or discrete parts of the spectrum—indicating that these transitions come from the highest spin states populated. (ii) Angular distribution measurements show predominantly a stretched quadrupole component in these decays. These characteristics can be explained by a model which assumes that the quadrupole bump is composed of collective transitions within rotational bands parallel to the yrast line. The effective moments of

inertia derived from the multiplicities and excitation energies of these transitions are close to the values for a rigid rotor. However, until now no measurements have shown that these transitions are indeed very highly collective. In the present experiment an attempt is made to measure average lifetimes in the bump region by a Doppler-shift method.

The experimental setup is similar to the one described in Ref. 3, with six  $7.6 \times 7.6$ -cm<sup>2</sup> NaI detectors serving as a multiplicity filter. Two  $7.6 \times 7.6$ -cm<sup>2</sup> NaI detectors were located at 0° and 90° with respect to the beam direction at a distance of 60 cm from the target to allow for neutron discrimination. Average lifetimes of the continuum  $\gamma$  rays were deduced by comparing the Doppler shift for the spectra measured in the 0° detector with a thin self-supporting target and with a target on a thick backing.

The targets and compound nuclei studied using beams of 700-MeV <sup>136</sup>Xe from the Lawrence Berkeley Laboratory SuperHILAC are listed in Table I. In each case spectra were measured for an  $\sim 1$ -mg/cm<sup>2</sup> self-supporting target and for a target of similar thickness on a 25-mg/cm<sup>2</sup> Au backing. In order to keep the conditions as equal as possible for the two spectra, a 25-mg/cm<sup>2</sup> Au foil was placed  $\sim 2$  mm downstream from the thin foil targets. In addition, for the <sup>27</sup>Al + <sup>136</sup>Xe system, targets with Pb backings were used. In this case the stopping time is almost 2 times longer than in the Au stopper; this provides a check on

TABLE I. Intrinsic quadrupole moments  $Q_0$ , enhancement factors  $B(E2)/B(E2)_w$ , and deformation parameters  $\beta_2$  for the  $^{163}\text{Ho}^*$  and  $^{164}\text{Er}^*$  compound systems.

Target	Compound nucleus	Stopper	$ Q_0 $		Average	$\frac{B(E2)}{B(E2)_w}$	$\beta_2$
$^{27}\text{Al}$	$^{163}\text{Ho}^*$	Au	9.3(2.5) <sup>a</sup>	8.0(2.3) <sup>b</sup>	8.2(2.2)	270(100)	0.37(11)
$^{27}\text{Al}$	$^{163}\text{Ho}^*$	Pb	7.0(2.6) <sup>a</sup>	8.6(3.0) <sup>b</sup>			
$^{28}\text{Si}$	$^{164}\text{Er}^*$	Au	8.5(3.0) <sup>a</sup>	8.6(3.0) <sup>b</sup>	9.8(3.3)	380(180)	0.43(15)
$^{28}\text{Si}$	$^{164}\text{Er}^*$	Au	12.2(4.9) <sup>a</sup>	10.2(4.3) <sup>b</sup>			

<sup>a</sup>Determined from ratios of spectra at  $0^\circ$  as described in the text.

<sup>b</sup>Determined from double ratios of spectra at  $0^\circ$  and  $90^\circ$  as described in the text.

the reliability of the method as discussed below.

As an example of our data, Fig. 1(a) shows the sum of the twofold to sixfold spectra<sup>3</sup> obtained in the  $0^\circ$  detector for the self-supporting  $^{27}\text{Al}$  and the  $^{27}\text{Al}$  on Au targets. Below  $\sim 600$  keV, the displacement of the two spectra results mainly from lifetimes of the discrete lines. In the region of 750–1500 keV, the lifetimes of the continuum  $\gamma$  rays are responsible for the difference between the two spectra. At still higher  $\gamma$ -ray energies, the lifetimes are much shorter than the characteristic stopping time; hence, no difference is observed between the backed and the unbacked targets. The different effects in these three regions are accentuated in the ratio of the two spectra which is displayed in Fig. 1(b). The ratio for a different target,  $^{28}\text{Si}$ , is shown in Fig. 1(d).

Two methods were used to normalize the spectra obtained from the backed and the self-supporting targets: (i) As was explained above, no difference is expected in the range of  $E_\gamma \gtrsim 2$  MeV; therefore, the two spectra were matched in this energy region. (ii) No Doppler shift is expected in the detector at  $90^\circ$ . Hence by taking the double ratio of spectra from the backed and from the self-supporting targets at  $0^\circ$  and  $90^\circ$  we were able to get a normalization which eliminates some of the possible systematic errors, at the expense of a larger statistical uncertainty.

The data were analyzed in the following way. First the pulse-height spectra were unfolded<sup>4</sup> to give the primary photon spectra. The spectrum for recoil into vacuum was then folded with the response function calculated for a Doppler-shifted distribution, and the calculated ratio of spectra for recoil into vacuum and for recoil into backing was compared to the experimental ratio. It should be noted that the theory provides only

the Doppler response function. The result of convoluting the experimental spectra with the response function does not smooth the fluctuations in the original spectra as can be seen in Fig. 1(c).

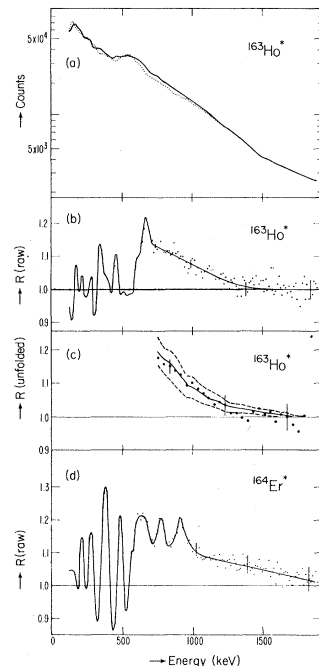


FIG. 1. (a) Sum of twofold to sixfold coincidence  $\gamma$ -ray spectra (raw data) measured at  $0^\circ$  for a self-supporting  $^{27}\text{Al}$  target (solid curve) and for a  $^{27}\text{Al}$  target on a Au backing (dotted curve). (b) Ratio of the raw (not unfolded) spectra measured at  $0^\circ$  for a self-supporting  $^{27}\text{Al}$  target and a  $^{27}\text{Al}$  target on a Au backing (the curve is drawn to guide the eye). (c) Ratio of the unfolded spectra (dots) measured at  $0^\circ$  for a self-supporting  $^{27}\text{Al}$  target and for a  $^{27}\text{Al}$  target on a Au backing. The solid curve represents the best fit of the calculated ratio to the data. The dashed lines show the ratios calculated for the two extreme values of  $Q_0$  allowed by the errors given in Table I. (d) Same as in (b), but for a  $^{28}\text{Si}$  target.

The response function which generates the Doppler-broadened spectrum was obtained by following the population of the decaying levels during the slowing down of the emitting nuclei. The population of levels in the continuum was calculated using a model in which the continuum is described by a series of rotational bands with an average moment of inertia  $\mathcal{J}$ . To each energy bin at a median energy  $E_\gamma$  a spin  $I$  is assigned using the relationship  $E_\gamma = (\hbar^2/2\mathcal{J})(4I-2)$  with the empirical<sup>3,5</sup> value  $2\mathcal{J}/\hbar^2 = 150 \pm 20 \text{ MeV}^{-1}$ . We assume that the level decays to the next member of the band by an  $E2$  transition. The feeding of each level consists of two parts: the prompt feeding, and the cascading from upper members of the band. The prompt part is approximated by a  $\sigma_I$ -distribution of initial populations,<sup>2</sup>  $\sigma_I \propto I/1 + \exp[(1 - I_{\text{max}})/2.5]$ , where  $I_{\text{max}}$  is the maximum angular momentum brought into the compound nucleus, determined for this case as  $I_{\text{max}} = 50$ . For the cascading part, the transition lifetimes are determined according to the rotational model with a constant intrinsic quadrupole moment  $Q_0$ ,<sup>6,7</sup> so that

$$\tau = (8 \times 10^2) E^{-5} (\text{keV}) \times (\langle I_i 2I_f K | I_i 2I_f K \rangle^2 e^2 Q_0(b)^2)^{-1} \text{ sec.}$$

The population equations are solved for all members of the band which contribute to the feeding. To solve this system of 10–30 coupled linear equations, we derived a fast algorithm which made the analysis of the experiment tractable. The slowing-down process was calculated using the Northcliffe and Schilling<sup>8</sup> electronic stopping power and the nuclear contribution was treated according to Blaugrund.<sup>9</sup>

The average  $Q_0$  is obtained by fitting the calculated ratios of the spectra for the backed and unbacked targets to the experimental ratio with  $Q_0$  as the only free parameter. The  $Q_0$  values, corresponding enhancement factors (in Weisskopf units<sup>6</sup>), and deformation parameters<sup>7</sup> obtained for the two systems investigated are given in Table I. Figure 1(c) shows the ratio of the unfolded spectra measured at  $0^\circ$  for a Au-backed and unbacked  $^{27}\text{Al}$  target in the region of interest. The solid line is the best-fitting calculated curve. The dashed lines show the ratios calculated for the two extreme values of  $Q_0$  allowed by the errors given in Table I.

The uncertainties assigned to the results contain estimates of the following systematic errors: (i) neglect of terms higher than first order in

$v/c$ , of angular distribution effects due to hyperfine interaction (the deorientation effect is calculated to be insignificant), and of finite target thickness (we assume no transverse velocity even at the range of nuclear stopping); (ii) uncertainty from insufficient knowledge of the stopping power; (iii) an estimated fivefold increase in the statistical errors from unfolding the raw data.

There is a small amount of statistical  $\gamma$  rays present in the bump region of the spectrum. Angular correlation experiments show,<sup>3</sup> however, that the bump region consists of  $\sim 90\%$  quadrupole radiation in these heavy rare-earth nuclei. Furthermore, since the sensitivity of the method depends on the slope of the spectrum, and the slope of the statistical part of the spectrum is much less steep than that of the bump, our method is less sensitive to the lifetime of the statistical  $\gamma$  rays.

With a moment-of-inertia parameter of  $2\mathcal{J}/\hbar^2 = 150 \text{ MeV}^{-1}$  we can correlate a spin range of  $I = 30\text{--}50$  to the  $\gamma$ -ray energy region of 0.8 to 1.4 MeV, in which we observe a measurable effect. We derive from the data that the transitions between these high-spin states show an enhancement of  $\sim 300$  single-particle units and a rather large deformation of  $\beta_2 = 0.4$ . The latter value is consistent with the moment of inertia observed in Refs. 2, 3, and 5. We conclude that the transitions in the  $E2$  bump are of strongly collective nature, with as high or higher a degree of collectivity as in the ground-state rotational bands of deformed nuclei.

As can be seen from Fig. 1(c) there is good agreement in both magnitude and slope for the calculated and measured curves. This indicates that for the investigated nuclei the model provides a satisfactory description of their behavior, suggesting no abrupt change in structure in the investigated region. Changes in structure corresponding to different lifetimes can give rise to regions where the fit with a single value of  $Q_0$  is not good. This may provide a method for studying nuclear-structure changes in the continuum region.

We would like to thank Dr. D. Ward for helpful discussions on the stopping-power calculations. One of us (H.H.) acknowledges receipt of a Max Kade Foundation Fellowship. Another (B.H.) acknowledges partial financial support by the Danish Natural Science Research Council.

<sup>(a)</sup>Permanent address: Institut für Strahlen- und Kernphysik, D-5300 Bonn, W. Germany.

<sup>(b)</sup>Permanent address: Department of Physics, The Weizmann Institute of Science, Rehovot, Israel.

<sup>1</sup>R. S. Simon, M. V. Banaschik, R. M. Diamond, J. O. Newton, and F. S. Stephens, Nucl. Phys. A290, 253 (1977).

<sup>2</sup>M. A. Deleplanque, I. Y. Lee, F. S. Stephens, R. M. Diamond, and M. M. Aleonard, Phys. Rev. Lett. 40, 629 (1978).

<sup>3</sup>M. A. Deleplanque, Th. Byrski, R. M. Diamond, H. Hübel, F. S. Stephens, B. Herskind, and R. Bauer, to be published.

<sup>4</sup>J. F. Mollenauer, Phys. Rev. 127, 867 (1962).

<sup>5</sup>D. Hillis, B. Fernandez, F. Folkmann, J. Garrett, G. B. Hagemann, and B. Herskind, to be published.

<sup>6</sup>A. Bohr and B. R. Mottelson, *Nuclear Structure* (Benjamin, New York and Amsterdam, 1969), Vol. I, p. 389.

<sup>7</sup>K. Alder and A. Winther, *Coulomb Excitation* (Academic, New York and London, 1966).

<sup>8</sup>L. C. Northcliffe and R. F. Schilling, Nucl. Data, Sect. A 7, 233 (1970).

<sup>9</sup>A. E. Blaugrund, Nucl. Phys. 88, 591 (1966).

## Can Pions Be Strongly Bound in Nuclei?

E. Friedman, A. Gal, and V. B. Mandelzweig

*The Racah Institute of Physics, The Hebrew University of Jerusalem, Israel*

(Received 21 July 1978)

On the basis of new data on pionic atoms, it is argued that the criticality condition for the existence of strongly bound  $\pi$ -nuclear states is likely to be met in most nuclei. Numerical solutions for  $^{27}\text{Al}$ ,  $^{48}\text{Ca}$ , and  $^{209}\text{Bi}$  are reported, with the conclusion that the widths of such  $\pi$  states are generally prohibitively large for their observability except, possibly, in heavy nuclei.

The possible existence of pion-nuclear strongly bound states has recently been suggested by Ericson and Myhrer<sup>1</sup> (EM) who noted that the  $p$ -wave attractive term  $\nabla\alpha(r)\cdot\nabla$ , with  $\text{Re}\alpha(r) > 0$ , in the pion-nuclear optical potential may overcome the pion kinetic energy, thus leading to an infinity of strongly bound states. While a criticality condition must be met for such states to exist mathematically, it is by no means clear that their strong-interaction widths are not prohibitively large for any conclusive observation. Also, it was concluded by EM, on the basis of a particular parametrization<sup>2</sup> of the optical potential, that the criticality condition is not met in most ordinary nuclei.

In this Letter we point out that the new precise

data<sup>3</sup> on  $2p$  levels in pionic atoms (Al to Zn) lead to a different parametrization [procedure (b) of Ref. 3] of the pion-nuclear zero-energy optical potential, for which the criticality condition is satisfied in many nuclei. This parametrization also reproduces<sup>4</sup> all existing data for  $1s$  states. We report here numerical results for pionic bound states in the representative nuclei  $^{27}\text{Al}$ ,  $^{48}\text{Ca}$ , and  $^{209}\text{Bi}$  and mention the far-reaching consequences of nuclear absorption on these states.

The pion-nuclear low-energy potential is given by

$$2\mu V(r) = q(r) + \nabla\alpha(r)\cdot\nabla, \quad (1)$$

where  $q(r)$  is the local ( $s$ -wave) part which for  $\pi^-$  reads

$$q(r) = 4\pi\left\{(1 + \mu/m)[b_0(\rho_n + \rho_p) + b_1(\rho_n - \rho_p)] + (1 + \mu/2m)B_0 4\rho_p\rho_n\right\}, \quad (2)$$

$\mu$  and  $m$  being the pion-nucleus reduced mass and the nucleon mass, respectively.  $B_0$  is a complex number, simulating both dispersive and absorptive effects ignored by the first-order term.  $\rho_{p,n}$  are the nuclear densities. The nonlocal ( $p$ -wave) part is parametrized here as follows:

$$\alpha(r) = \frac{\alpha_0(r)}{1 + \xi \frac{1}{3}\alpha_0(r)} + 4\pi \left(1 + \frac{\mu}{2m}\right)^{-1} C_0 4\rho_p\rho_n, \quad 0 \leq \xi \leq 1, \quad (3a)$$

$$\alpha_0(r) = 4\pi(1 + \mu/m)^{-1}[c_0(\rho_n + \rho_p) + c_1(\rho_n - \rho_p)], \quad (3b)$$

where  $C_0$ , again, is a complex number. The strength  $\xi$  of the Lorentz-Lorenz (LL) renormalization is at present, not uniquely determined by pionic-atom data.

In the absence of compelling theoretical motivation, the two-nucleon term of Eq. (3a) is stripped of its customary LL renormalization. This results in a value for  $C_0$  which differs from the value report-